the plant journal

SEB Society for Experimental Biology

The Plant Journal (2014) **80,** 745–757 doi: 10.1111/tpj.12674

FEATURED ARTICLE

High lipid order of Arabidopsis cell-plate membranes mediated by sterol and DYNAMIN-RELATED PROTEIN1A function

Márcia Frescatada-Rosa[1,†], Thomas Stanislas[1,†], Steven K. Backues[2,‡], Ilka Reichardt[3,§], Shuzhen Men[1,¶], Yohann Boutté[1,], Gerd Jürgens[3], Thomas Moritz[4], Sebastian Y. Bednarek[2] and Markus Grebe[1,5,*]**

[1]*Department of Plant Physiology, Umeå Plant Science Centre, Umeå University, SE-90187 Umeå, Sweden,*

[2]*Department of Biochemistry, University of Wisconsin-Madison, Madison, WI 53706, USA,*

[3]*Department of Developmental Genetics, Centre for Plant Molecular Biology, University of Tübingen, Auf der Morgenstelle 3, D-72076 Tübingen, Germany,*

[4]*Department of Forest Genetics and Plant Physiology, Umeå Plant Science Centre, Swedish University of Agricultural Sciences, SE-90183 Umeå, Sweden, and*

[5]*Institute for Biochemistry and Biology, Plant Physiology, University of Potsdam, Karl Liebknecht Straße 24-25, Building 20, D-14476 Potsdam-Golm, Germany*

Received 3 May 2014; revised 21 August 2014; accepted 4 September 2014; published online 18 September 2014.

*For correspondence (e-mail markus.grebe@uni-potsdam.de).

†These authors contributed equally to this work.

‡Present address: 6036 Life Sciences Institute, University of Michigan, 210 Washtenaw Avenue, Ann Arbor, MI 48109-2216, USA.

§Present address: Institute of Molecular Biotechnology of the Austrian Academy of Sciences, Dr Bohr Gasse 3, A-1030 Vienna, Austria.

¶Present address: College of Life Sciences, Nankai University, 94 Weijin Road, Nankai District, Tianjin 300071, China.

**Present address: Membrane Biogenesis Laboratory, UMR 5200 CNRS, Université Bordeaux Segalen Bâtiment A3, INRA Bordeaux Aquitaine BP81, 71 Avenue Edouard Bourlaux, 33883 F-Villenave d'Ornon, France.

SUMMARY

Membranes of eukaryotic cells contain high lipid-order sterol-rich domains that are thought to mediate temporal and spatial organization of cellular processes. Sterols are crucial for execution of cytokinesis, the last stage of cell division, in diverse eukaryotes. The cell plate of higher-plant cells is the membrane structure that separates daughter cells during somatic cytokinesis. Cell-plate formation in Arabidopsis relies on sterol- and DYNAMIN-RELATED PROTEIN1A (DRP1A)-dependent endocytosis. However, functional relationships between lipid membrane order or lipid packing and endocytic machinery components during eukaryotic cytokinesis have not been elucidated. Using ratiometric live imaging of lipid order-sensitive fluorescent probes, we show that the cell plate of *Arabidopsis thaliana* represents a dynamic, high lipid-order membrane domain. The cell-plate lipid order was found to be sensitive to pharmacological and genetic alterations of sterol composition. Sterols co-localize with DRP1A at the cell plate, and DRP1A accumulates in detergent-resistant membrane fractions. Modifications of sterol concentration or composition reduce cell-plate membrane order and affect DRP1A localization. Strikingly, DRP1A function itself is essential for high lipid order at the cell plate. Our findings provide evidence that the cell plate represents a high lipid-order domain, and pave the way to explore potential feedback between lipid order and function of dynamin-related proteins during cytokinesis.

Keywords: membrane order, sterol, cytokinesis, DRP1A, Arabidopsis.

INTRODUCTION

Cytokinesis represents the final stage of cell division during which the cytoplasm of a single cell is partitioned to form two daughter cells. A number of differences may be observed during cytokinesis of various eukaryotes (Jürgens, 2005; Barr and Grüneberg, 2007; Prekeris and Gould, 2008). However, similarities include the requirement for membrane fusion to occur at diverse cytokinetic structures, for example at the animal mid-body or the plant cell plate (Jürgens, 2005; Barr and Grüneberg, 2007; Prekeris and Gould, 2008). Precise execution of cytokinesis relies on the correct composition of membrane lipids, including, among others, eukaryotic membrane sterols

(Wachtler *et al.*, 2003; Fernandez *et al.*, 2004; Men *et al.*, 2008; Boutté *et al.*, 2010). The plant cell plate is a transitory membrane compartment whose biogenesis requires fusion of mostly *trans*-Golgi network-derived secretory vesicles in the plane of cell division (Samuels *et al.*, 1995; Jürgens, 2005). Vesicle fusion is accomplished by SNARE complex machineries, of which the KNOLLE syntaxin is a critical component localized to the cell plate (Lauber *et al.*, 1997). Expansion of the early cell plate and the final fusion of the late cell plate with the parental plasma membrane complete separation of daughter cells during cytokinesis of somatic plant cells (Jürgens, 2005). Cell-plate formation in Arabidopsis relies on sterol- and DYNAMIN-RELATED PROTEIN1A (DRP1A)-dependent endocytosis (Collings *et al.*, 2008; Men *et al.*, 2008; Boutté *et al.*, 2010). Dynamin also accumulates at mid-body membranes during animal cytokinesis (Skop *et al.*, 2004). In addition to DRP1A, other members of the DRP1 family of *Arabidopsis thaliana* that contribute to clathrin-mediated endocytosis (CME) are enriched at the cell plate (Kang *et al.*, 2003a,b; Fujimoto *et al.*, 2007, 2008) and co-localize with the clathrin light chain (CLC) at the plasma membrane as well as the cell plate (Konopka and Bednarek, 2008a; Fujimoto *et al.*, 2010). The internalization from the cell plate of cargo molecules such as KNOLLE (Boutté *et al.*, 2010), which is enriched in clathrin-coated vesicles (McMichael *et al.*, 2013), as well as removal of the PIN2 auxin efflux carrier from the basal epidermal plasma membrane after cytokinesis, requires sterol-dependent endocytosis via a clathrin- and DRP1A-mediated mechanism (Collings *et al.*, 2008; Men *et al.*, 2008; Boutté *et al.*, 2010; Mravec *et al.*, 2011). Sterols are required for correct execution of cytokinesis in diverse eukaryotes (Wachtler *et al.*, 2003; Fernandez *et al.*, 2004; Men *et al.*, 2008). Sterols accumulate in the septum during cytokinesis of the fission yeast *Schizosaccharomyces pombe* as well as in the cytokinetic furrow of the sea urchins *Strongylocentrotus drobachiensis* and *Lytechinus pictus* (Wachtler *et al.*, 2003; Takeda *et al.*, 2004; Ng *et al.*, 2005), and the latter has been suggested to be associated with high lipid-order membrane domains (Ng *et al.*, 2005). Similarly, the mammalian mid-body is thought to represent a sterol-enriched membrane during final stages of mammalian cytokinesis (Skop *et al.*, 2004), but this has not been demonstrated. The mid-body has recently been found to accumulate specific lipids at high levels, including ceramides, triacylglycerol, phosphatidic acid and phosphatidylserine (Atilla-Gokcumen *et al.*, 2014). A high degree of lipid packing, also referred to as high membrane lipid order, is a biophysical feature of membrane rafts (Pike, 2006; Simons and Sampaio, 2011). Lipid order may be probed using fluorescent, lipid order-sensitive probes, both in artificial membranes *in vitro* (Jin *et al.*, 2006; Owen *et al.*, 2006) and in live cells *in vivo* (Owen *et al.*, 2012). The fluorescent probe di-4-ANEPPDHQ has been validated for determining lipid order in extracted plant membranes and in live imaging of plant cells (Roche *et al.*, 2008; Liu *et al.*, 2009; Gerbeau-Pissot *et al.*, 2013). Lipid order affects the fluorescence emission spectrum of di-4-ANEPPDHQ, with the spectral region between 500 and 580 nm representing the ordered phase of the membrane, and fluorescence between 620 and 750 nm representing the disordered phase (Owen *et al.*, 2012). The degree of membrane lipid order may thus be quantified by ratiometric imaging and subsequent calculation of the generalized polarization (GP) value (Owen *et al.*, 2012). Here, we combine di-4-ANEPPDHQ-based live imaging of lipid order, cell biological visualization of sterols and cell-plate proteins, and biochemical as well as functional genetic analyses to elucidate the relationship between membrane order, sterol content and DRP1A function in plant cytokinesis. Our results reveal that the plant cell plate is a high lipid-order membrane domain whose lipid order strictly relies on correct sterol composition and DRP1A protein function.

RESULTS

The cell plate is a dynamic, high lipid-order membrane domain

In order to explore potential differences in lipid order between membranes in plant roots, we employed ratiometric live imaging using the fluorescent lipid-order probe di-4-ANEPPDHQ to study root epidermal cells of Arabidopsis seedlings. We monitored two regions of the emission spectrum of this probe, reflecting the ordered and disordered phases (Figure 1a), to generate ratiometric pseudo-colored GP images, in which red and green correspond to high or low GP values reflecting higher and lower membrane lipid order, respectively (Figure 1b). Intriguingly, the cell plate of meristematic cells consistently displayed a higher GP value than the plasma membrane of wild-type seedlings (Figure 1b), which we confirmed by quantitative and statistical analyses of GP values from the cell plate and the plasma membrane at the single-cell level (Figure 2a). Furthermore, analyzing GP values from cell plates at various cytokinetic stages (early stage, middle stage and late stage, $n = 15$ for each stage) indicated a progressive decrease in cell-plate lipid order, but the lipid order of the plasma membrane did not change during cytokinesis (Figure 2b,c and Tables S1, S2 and S3). In addition, we calculated the GP values for the cell plate relative to the GP value of the closest plasma membrane, and noticed a progressive decrease in the relative GP values from early to middle and late stages, with the relative GP values from early and late stages being highly significantly different (Figure 2d and Table S1). Consistent with these findings, following individual cells over time by ratiometric imaging of GP values throughout cell-plate maturation revealed a dynamic

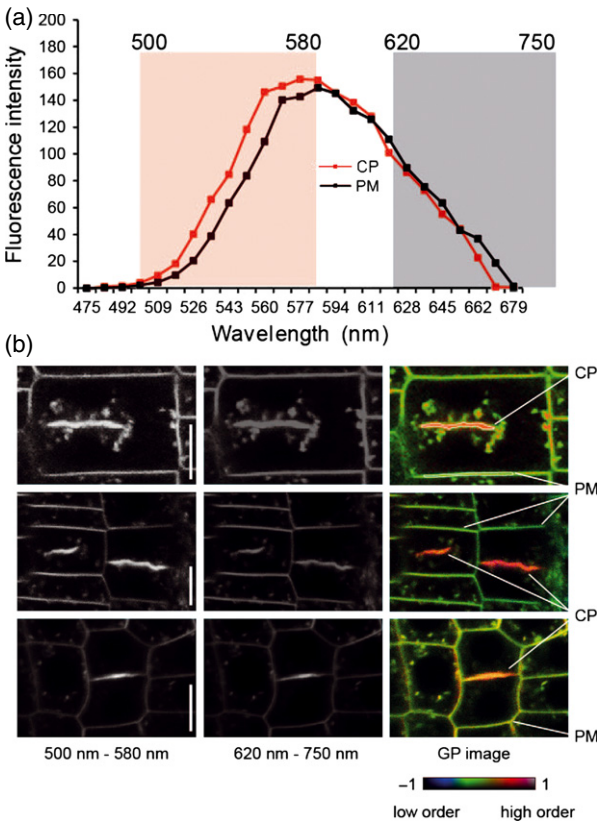

Figure 1. The cell plate is a high lipid-order membrane domain.
Ratiometric fluorescence live imaging analysis of membrane lipid order in cytokinetic cells from 5-day-old *Arabidopsis thaliana* seedling roots labeled with the lipid order-sensitive probe di-4-ANEPPDHQ.
(a) Fluorescence properties of di-4-ANEPPDHQ. The dye is excited using a 488 nm laser. The red line corresponds to the spectrum of the dye at the cell plate (CP), whereas the black line corresponds to the spectrum at the plasma membrane (PM). Two-channel acquisition is performed in the wavelength bands indicated by red shading (500–580 nm) and gray shading (620–750 nm).
(b) Left panels: di-4-ANEPPDHQ fluorescence recorded between 500–580 nm, representing high lipid order. Middle panels: fluorescence recorded at 620–750 nm representing low lipid order. Right panels: ratiometric color-coded GP images obtained after processing images recorded at 500–580 and 620–750 nm as described previously (Owen *et al.*, 2012) and in the Experimental procedures. Red, high lipid order; black, low lipid order.

decrease in cell-plate lipid order, while lipid order of the plasma membrane remained fairly constant (Figure 2e,f).

The cell plate is a sterol-sensitive, high lipid-order membrane domain

We confirmed the high lipid order of the cell plate by quantitative analyses of GP values from cell plates and plasma membranes from large populations of cytokinetic cells obtained from multiple experiments (Figure 3c and Tables S2 and S3). We used a recently developed membrane lipid order probe, PY3174 (Kwiatek *et al.*, 2013), in live-cell imaging, and observed higher GP values for cell plates than for plasma membranes of cytokinetic cells (Figure S1 and Table S2), very similar to the results obtained with di-4-ANEPPDHQ. Together, these findings strongly suggest that the cell plate represents a high lipid-order membrane domain.

We next assessed whether modifications of the membrane sterol content affect the lipid order of cell-plate membranes. Membrane order may be modified by the concentration and molecular nature of the sterols integrated into the phospholipid bilayer (Xu *et al.*, 2001; Jin *et al.*, 2006; Owen *et al.*, 2006; Roche *et al.*, 2008). Genetic and pharmacological tools allow modulation of sterol concentration and composition in plants. For example, seedlings defective in the sterol biosynthesis gene *CYCLOPROPYLSTEROL ISOMERASE1* (*CPI1*), or treated with the sterol biosynthesis inhibitor fenpropimorph (fen), display a substantially modified sterol profile, primarily accumulating cyclopropylsterols (He *et al.*, 2003; Men *et al.*, 2008). We also observed a strong shift of the sterol profile towards cyclopropylsterols in *cpi1-1* mutant root callus, although the callus retained a significant amount of sitosterol (Figure 4a), which was found to be almost completely absent in seedling roots (Men *et al.*, 2008). The sterol biosynthesis inhibitor lovastatin (lov) inhibits the activity of 3-hydroxy-3-methylglutaryl CoA reductase, causing a reduction of total sterol concentration (Bach and Lichtenthaler, 1983). Treatment of Arabidopsis seedlings with 1 μM lov or 50 μg ml^{-1} fen significantly reduced the total amount of sterols or converted a large proportion of sterols into cyclopropylsterols, respectively (Figure 4b). We used the *cpi1-1* mutant and inhibitor treatments to address whether interference with sterol biosynthesis affects membrane order as visualized by ratiometric di-4-ANEPPDHQ imaging. Intriguingly, the GP values for cell plates and plasma membranes of individual cells (Figure 3a) and from large populations of cytokinetic cells were similar for cytokinetic cells of the *cpi1-1* mutant (Figure 3b,c and Tables S2 and S3), as well as fen-treated wild-type roots (Figure 3b,c and Tables S2 and S3). Cells from roots treated with lov also displayed significantly lower GP values at the cell plate compared with the dimethylsulfoxide (DMSO)-treated control (Figure 3c). This is in contrast to the strikingly higher GP values observed for the cell plates of wild-type cells or solvent-treated control cells compared to their plasma membranes (Figure 3b,c and Table S3). Thus, our results strongly suggest that the cell plate represents a dynamic, high lipid-order membrane domain that is highly sensitive to alterations in sterol concentration or composition.

DRP1A and other CME components are enriched in detergent-resistant membranes and co-localize with sterols at the cell plate

Membrane rafts act as platforms at which specific proteins assemble through cooperative interactions between proteins, sterols and sphingolipids (Pike, 2006; Simons and Sampaio, 2011). A biochemical tool to estimate the

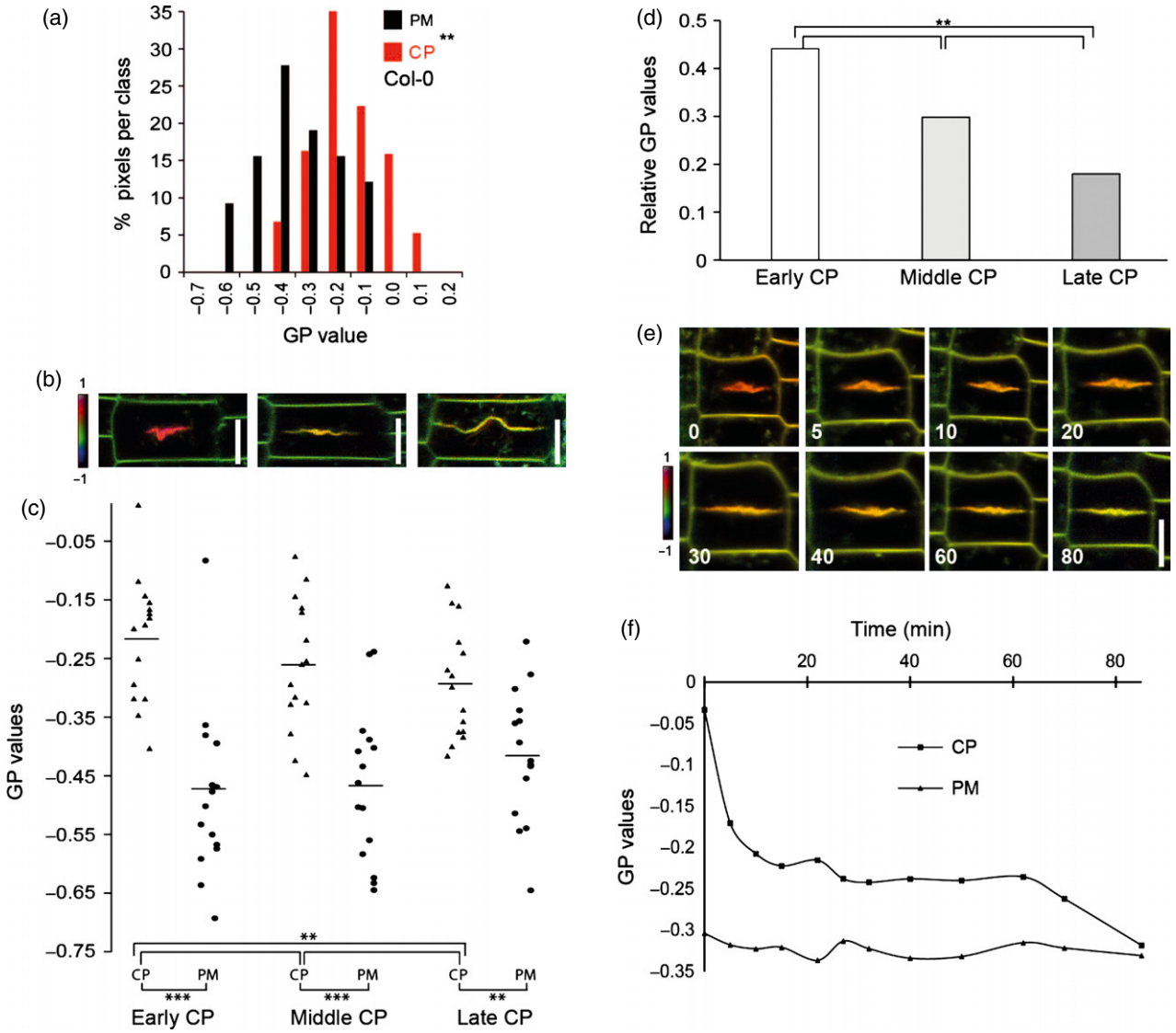

Figure 2. Dynamics of high lipid order at the cell plate during cytokinesis.
(a) Histograms showing the percentage of pixels per class of GP values between -0.7 (lower order) and 0.2 (higher order). Values were extracted from a single cell plate (CP) and the closest plasma membrane (PM) of a cytokinetic Col-0 cell. Note the significant shift of GP values at the CP towards higher order compared to GP values at the PM. Asterisks indicate a statistically significant difference between the GP value distributions for the PM and for the CP (**$P = 0.0011$).
(b) GP images of representative cytokinetic stages (early CP, middle CP and late CP) in Col-0. Note the decrease in lipid order (from red to yellow) from early to late CPs, while the PM order remains lower (green).
(c) Quantitative analysis of mean GP value distributions for CPs and PMs obtained from multiple cells of the early, middle and late cytokinetic stages shown in (b). Fifteen cells were analyzed per stage. The horizontal lines indicate the means of the non-normal distributions. *P* values obtained using the non-parametric, two-tailed Mann–Whitney test indicate that differences between the distributions are highly significant (***$P < 0.001$) or significant (**$P < 0.005$). Exact *P* values are given in Table S2.
(d) Mean relative GP values for each individual cell from the three cytokinetic stages from (c) calculated using the equation $(GP_{PM} - GP_{CP})/(GP_{PM} + GP_{CP})$. Fifteen cells were analyzed per stage. *P* values obtained using Student's two-tailed *t* test for two samples indicate that differences between the distributions are significant (**$P < 0.01$). Exact *P* values are given in Table S1.
(e) Time series of membrane order represented by eight selected GP images of a cell throughout the various stages of cell-plate formation. Numbers indicate the time (min) from onset of imaging of an early unfused cell plate until cell-plate fusion.
(f) Quantification of all GP values extracted from the CP and PM for all 12 images acquired during the time series.
Scale bars = 5 μm.

abundance of proteins associated with sterol-enriched membrane domains involves preparation and extraction of proteins that co-fractionate in detergent-resistant membranes (DRMs) (Mongrand *et al.*, 2004; Borner *et al.*, 2005; Lingwood and Simons, 2007). To determine whether components of the CME machinery associate with DRMs from roots, DRMs were prepared from total membrane fractions obtained from *Arabidopsis thaliana* wild-type and

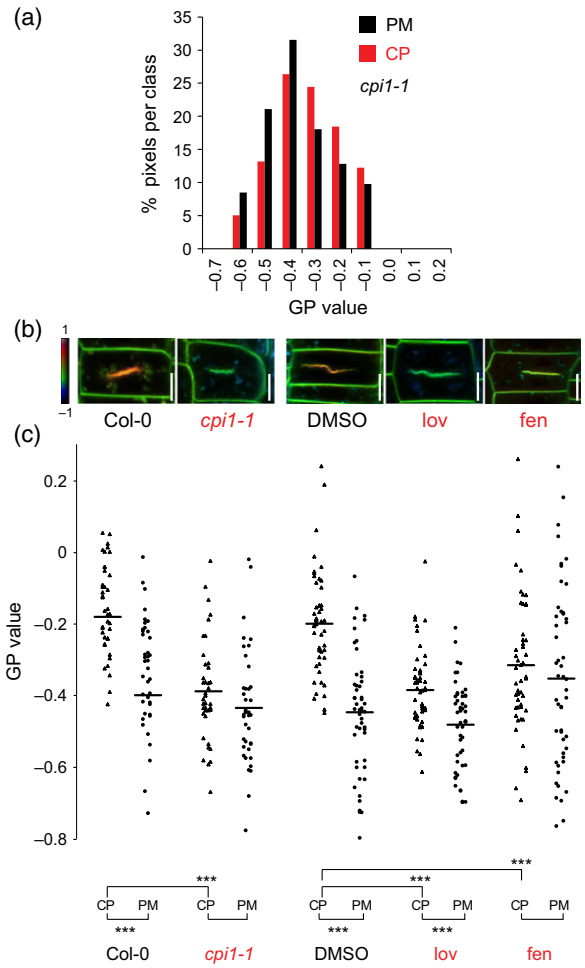

Figure 3. The high lipid order of cell-plate membranes is sterol-dependent.
(a) Histograms showing the percentage of pixels per class of GP values between -0.7 (lower order) and 0.2 (higher order). Values were extracted from a single cell plate (CP) and the closest plasma membrane (PM) of a cytokinetic *cpi1-1* cell (in the Col-0 background). There was no significant shift of GP values at the CP compared to GP values at the PM in *cpi1-1* ($P = 0.972$).
(b) GP images of representative cytokinetic cells of the genotypes or treatments: Col-0 (wild-type), *cpi1-1* in the Col-0 background (*cpi1-1*), Col-0 treated with 0.1% DMSO as a solvent control, Col-0 treated with 1 μM lovastatin (lov) and Col-0 treated with 50 μg ml^{-1} fenpropimorph (fen). Note the higher lipid order (orange/red) at the CP compared to the PM (green) in Col-0 (wild-type) and Col-0 treated with 0.1% DMSO compared to the lower lipid order at the CP and PM (green) in *cpi1-1* and lov- or fen-treated cells. Scale bars = 5 μm.
(c) Quantitative analysis of mean GP value distributions for CPs and PMs obtained from multiple cells of the genotypes or treatments shown in (b). Forty cells in three to ten imaging experiments were analyzed for Col-0 and *cpi1-1*, and 50 cells were analyzed for DMSO, lov and fen treatments. The horizontal lines indicate the means of the non-normal distributions. *P* values obtained using the non-parametric, two-tailed Mann–Whitney test indicate that differences between distributions are highly significant (**$P < 0.001$) or very highly significant (***$P < 0.0001$). Exact *P* values are given in Tables S2 and S3.

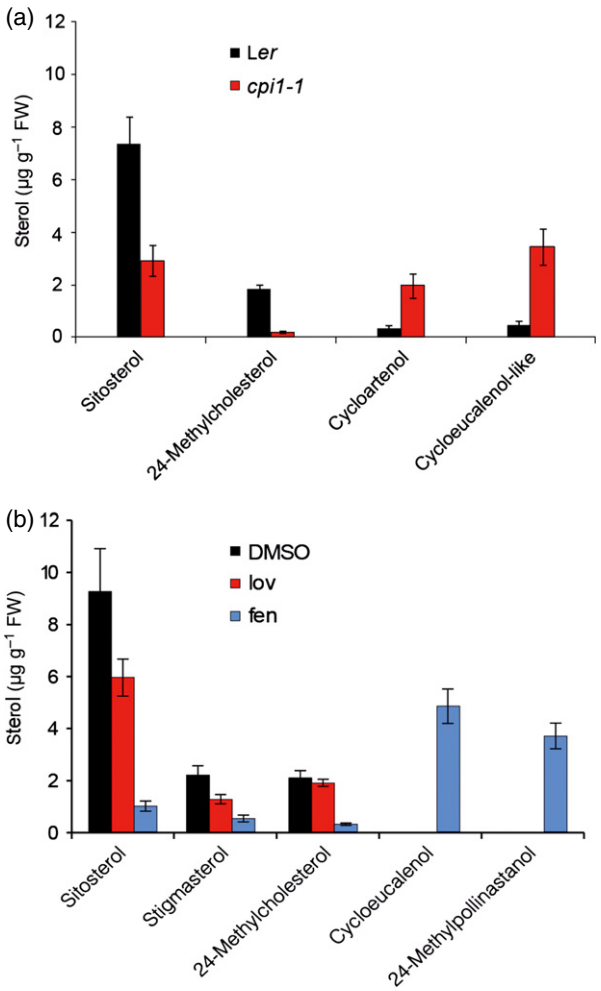

Figure 4. Altered sterol composition in *cpi1-1* mutant root callus and in roots treated with sterol biosynthesis inhibitors.
(a) GC/MS composition analysis of bulk sterols in 3-week-old root callus cultures generated from roots of L*er* wild-type and the homozygote *cpi1-1* mutant (in the L*er* background). Callus of individual cultures was pooled from callus collections at passage after 3 weeks of culture, when small callus pieces were transferred to fresh culture plates. Values are means ± SD obtained from $n = 4$ cultures of L*er* and $n = 8$ cultures of *cpi1-1* grown in parallel. Sterol composition is expressed as μg g^{-1} fresh weight of callus.
(b) GC/MS composition analysis of bulk sterols from 5-day-old Col-0 seedling roots obtained from seedlings grown on MS agar plates containing 0.1% DMSO (DMSO), 1 μM lovastatin (lov) or 50 μg ml^{-1} fenpropimorph (fen). Sterol composition is expressed as μg g^{-1} fresh weight. Values are means ± SD from five independent biological experiments. Note reduction of bulk sterol content for sitosterol, stigmasterol and 24-methylcholesterol (campesterol) upon lov treatment compared to the striking accumulation of the cyclopropylsterols cycloeucalenol and 24-methylpollinastanol upon fen treatment.

cpi1-1 mutant root callus cultures and analyzed by immunoblotting. This revealed that, in contrast to the DRM-depleted protein STEROL METHYLTRANSFERASE 1 (SMT1) (Boutté *et al.*, 2010), the CME components CLATHRIN HEAVY CHAIN (CHC), CLATHRIN LIGHT CHAIN (CLC), DRP1A (Kang *et al.*, 2003a; Fujimoto *et al.*, 2007, 2010; Konopka and Bednarek, 2008a; Kitakura *et al.*, 2011; Wang *et al.*, 2013) and ADP-RIBOSYLATION FACTOR1 (ARF1), which are required for endocytosis (Xu and Scheres, 2005; Boutté *et al.*, 2010), were enriched in DRMs obtained from both wild-type and *cpi1-1*-mutant callus (Figure 5a–d). Our

finding that DRMs from *cpi1-1* mutant callus showed levels similar to the wild-type callus may partly be due to the fact that the sterol composition profile of *cpi1-1* root callus (Figure 4a) was not as strongly altered as that of *cpi1-1*-mutant roots (Men *et al.*, 2008). Although we did not observe differences in DRM association of the tested CME proteins between the *cpi1-1*-mutant and wild-type root callus, our results clearly show that several CME components from Arabidopsis root cells preferentially associate with DRMs, indicating that they may associate with membrane rafts.

To assess co-localization of CME components with sterol-rich membranes in roots *in situ*, we used the 3-β-hydroxysterol-specific probe filipin III (Grebe *et al.*, 2003) to co-label fluorescent filipin–sterol complexes with DRP1A, DRP2B or CLC 2 fused to GFP (DRP1A–GFP, DRP2B–GFP or CLC2–GFP). We observed that sterols clearly co-localized with DRP1A–GFP (Figure 5e–g), DRP2B–GFP (Figure 5h–j) and CLC2–GFP (Figure 5k–m) at the cell plate. Additionally, CLC2–GFP and sterols co-localized in some intracellular compartments (Figure 5k–m), most likely the *trans*-Golgi network/early endosome (Ito *et al.*, 2012), whose membranes are sterol-enriched (Boutté *et al.*, 2010). Taken together, several CME components co-localized with sterols at the cell plate in the plane of cell division.

Cell-plate accumulation of DRP1A is sensitive to sterol composition

Interestingly, specific localization of the KNOLLE syntaxin in the plane of cell division relies on sterol-dependent endocytosis in a clathrin- and DRP1A-dependent manner (Boutté *et al.*, 2010). KNOLLE is constrained to the cell plate and to endomembrane compartments in wild-type, but is ectopically found at lateral plasma membranes of late cytokinetic cells in *cpi1-1* and *drp1a* mutants (Boutté *et al.*, 2010). We determined whether loss of function of the two individual *DRP2* genes or the two individual *CHC* genes also affects KNOLLE cell-plate localization. However, we did not observe a deviation of KNOLLE localization from that of the wild-type in *drp2a*, *drp2b*, *chc1* and *chc2* single mutants (Figure S2a–f). This may be due to the reported redundancy within these two gene families as indicated by early lethality of respective double mutants (Backues *et al.*, 2010; Kitakura *et al.*, 2011).

We next evaluated whether altered sterol composition affects the cell-plate localization of CME components. In wild-type roots, DRP1A mainly localized along and towards

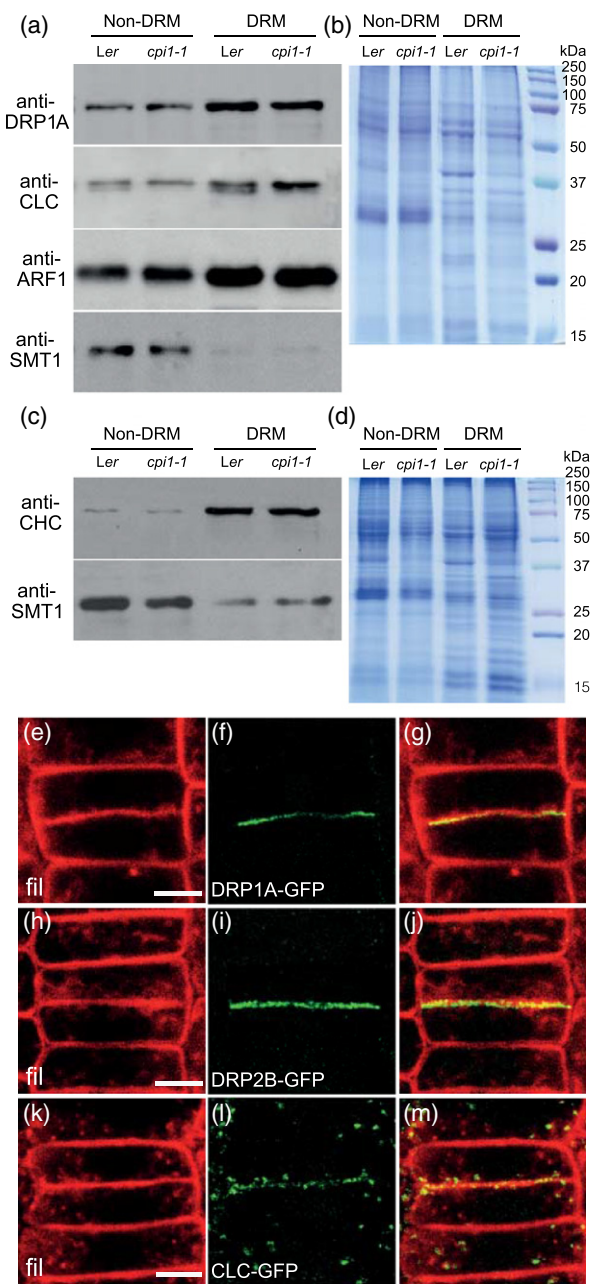

Figure 5. DRP1A is enriched in DRMs and co-localizes with sterols at the cell plate.
(a–d) Western blot analysis of DRM fractions from 3-week-old Arabidopsis callus cultures of wild-type L*er* and the *cpi1-1* mutant (in the L*er* background). Equal amounts of membrane protein were loaded from the control fraction mock-extracted at a Triton X-100 detergent/protein (w/w) ratio of 0 (non-DRM) and the DRM fraction extracted at a Triton X-100 detergent/protein (w/w) ratio of 8 (DRM). Similar results were obtained in three independent experiments.
(a) Western blot from DRM extractions probed with anti-DRP1A (isoform-specific), anti-CLC (generic), anti-ARF1 (generic) and anti-SMT1 (isoform-specific) antibodies.
(b) Replicate Coomassie Blue gel as a loading control for the blot in (a).
(c) Western blot from DRM extraction probed with anti-CHC (generic) and anti-SMT1 (isoform-specific) antibodies.
(d) Replicate Coomassie Blue gel as a loading control for the blot in (c).
The results in (a) and (c) indicate enrichment of DRP1A, CLC2, CHC and ARF1 in DRMs compared to depleted SMT1.
(e–m) Co-localization analyses at the cell plate in late cytokinetic cells: (e,h, k) filipin-sterol fluorescence (fil, red); (f) DRP1A–GFP, (i) DRP2B–GFP and (l) CLC2–GFP fluorescence (green). (g,j,m) Merged images of (e) and (f), (h) and (i), and (k) and (l), respectively. Scale bars = 5 μm.

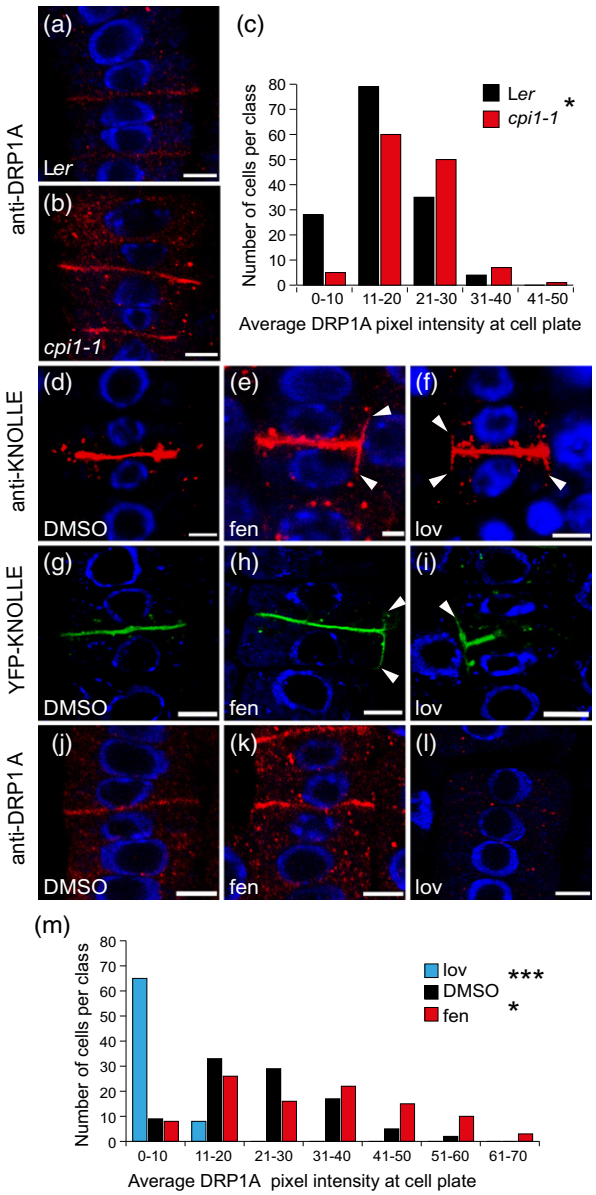

Figure 6. Cell-plate accumulation of DRP1A is sensitive to sterol composition.

(a,b) anti-DRP1A immunolocalization (red) in late cytokinetic root cells of (a) wild-type (L*er*) and (b) the *cpi1-1* mutant (in the L*er* background). Blue staining indicates DAPI-stained DNA.

(c) Quantification of DRP1A immunofluorescence intensity at cell plates from multiple cells (n = 125–146). Frequency distributions of cells per class average pixel intensity at the cell plate are shown. The mean pixel intensity was calculated as described in Experimental procedures. Non-normal distributions were analyzed for significance of differences between distributions by the non-parametric, two-tailed Mann–Whitney test with a significance threshold level of $P < 0.05$. The P value for L*er* (n = 146 cells from 50 roots) versus *cpi1-1* (n = 125 cells from 47 roots) is 0.014694 (asterisk).

(d–l) Analyses of 5-day-old root cells from Arabidopsis seedlings grown on medium supplemented with 0.1% DMSO solvent (d,g,j), 50 μg ml^{-1} fen (e,h,k) or 1 μM lov (f,i,l). (d–f) Anti-KNOLLE immunolabeling of late cytokinetic cells treated with (d) DMSO, (e) fen or (f) lov. (g–i) Functional YFP–KNOLLE expressed in late cytokinetic root cells of seedlings treated with (g) DMSO, (h) fen or (i) lov. Labeling of the ectopic lateral membrane by anti-KNOLLE (e,f) and YFP–KNOLLE (h,i) is indicated by arrowheads. (j–l) DRP1A immunofluorescence labeling of late cytokinetic root cells of seedlings treated with (j) DMSO, (k) fen or (l) lov. Blue staining indicates DAPI-stained DNA.

(m) Quantification of DRP1A immunofluorescence intensity at the cell plate from multiple cells of roots from seedlings treated with DMSO, fen or lov. Frequency distributions of cells per class average pixel intensity at the cell plate (calculated as described in Experimental procedures) are shown. Distributions were analyzed for significance of differences by the non-parametric, two-tailed Mann–Whitney test with a significance threshold level at $P < 0.05$. *P = 0.015068 for DMSO (n = 146 cells from 50 roots) versus fen (n = 100 cells from 31 roots); ***P < 2e-06 for DMSO (n = 95 cells from 25 roots) versus lov (n = 73 cells from 28 roots).

Scale bars = 5 μm in (a), (b) and (d–l).

the edges of the forming cell plate, and was also present in endomembrane compartments as well as at the plasma membrane (Figures 5f and 6a). In comparison with wild-type (Figure 6a), anti-DRP1A immunolabeling at the cell plate was enhanced in the *cpi1-1* mutant (Figure 6b), as corroborated by quantitative analysis of DRP1A immunofluorescence intensity at the plane of cell division (Figure 6c). In contrast, the cell-plate localization of DRP2B–GFP and CLC2–GFP appeared to be unaffected in cytokinetic *cpi1-1*-mutant cells (Figure S2g–r), possibly due to the abundance of other DRP2 and CHC isoforms at the cell plate, or due to a differential sterol sensitivity of these proteins compared to DRP1A.

Both genetic and pharmacological interference with membrane sterol composition induce mis-localization of KNOLLE at lateral plasma membranes during late cytokinesis (Boutté *et al.*, 2010). We obtained similar results for seedlings treated with 1 μM lov or with a lower fen concentration (50 μg ml^{-1}) than applied in previous studies (200 μg ml^{-1}) (Boutté *et al.*, 2010). When compared with solvent-treated wild-type (Figure 5d,g), fen and lov treatment induced lateral KNOLLE mis-localization (Figure 6e,f, h,i), under conditions that reduced cell-plate membrane lipid order (Figure 3b,c). We previously observed KNOLLE lateral mis-localization in the cyclopropylsterol-accumulating *cpi1-1* mutant; however, this did not strongly affect the rate of KNOLLE lateral diffusion (Boutté *et al.*, 2010). We also analyzed lateral diffusion of KNOLLE at the cell plate of DMSO-treated and lov-treated roots in the presence of the protein translation inhibitor cycloheximide and energy inhibitors (sodium azide and 2-deoxy-d-glucose) by fluorescence recovery after photobleaching (FRAP) analyses (Figure S3). Compared with cells from DMSO-treated roots (Figure S3a,c), functional YFP–KNOLLE displayed only marginally faster FRAP at cell plates from lov-treated roots (Figure S3b,c), suggesting that reduction of total sterol levels by lov treatment hardly affects lateral membrane diffusion of YFP–KNOLLE *per se*, similar to the results obtained for GFP–KNOLLE in the *cpi1-1* mutant (Boutté *et al.*, 2010). More strikingly, KNOLLE localization is strongly affected by interference with CME components, and particularly depends on DRP1A function (Boutté *et al.*, 2010). This prompted us to investigate whether sterol-modulated

membrane order may also affect DRP1A localization at the cell plate. Indeed, compared to solvent-treated control roots (Figure 6j), higher DRP1A immunofluorescence was found at the cell plate in fen-treated seedlings (Figure 6k); this result was supported by quantitative analysis (Figure 6m). In contrast, reducing sterol concentration by lov treatment strongly decreased the DRP1A signal (Figure 6l, m and Figure S2u,v). Similarly, Western blot analysis of total protein extracts revealed increased DRP1A protein levels in fen-treated seedlings compared to DMSO-treated controls, in contrast to the decreased DRP1A protein levels observed upon lov treatment (Figure S4). Taken together, our findings reveal differential effects of alterations in sterol composition and concentration on DRP1A localization at the cell plate.

DRP1A is required for high membrane lipid order at the cell plate

Previous studies showed that *DRP1A* and *CPI1* function is required for correct execution of cytokinesis and for endocytosis of cargo proteins such as KNOLLE during late cytokinesis (Boutté *et al.*, 2010) or the PIN2 auxin efflux carrier after cytokinesis, respectively (Men *et al.*, 2008; Mravec *et al.*, 2011). Moreover, analysis of the *drp1a cpi1-1* double mutant revealed a strong synergistic interaction of the *DRP1A* and *CPI1* genes (Boutté *et al.*, 2010). As interference with sterol composition and membrane order affected the cell-plate localization of DRP1A, we determined whether DRP1A contributes to membrane lipid order as visualized by di-4-ANEPPDHQ. In striking contrast to the wild-type, which exhibited a higher mean GP value for the cell plate than for the plasma membrane, cytokinetic cells in *drp1a*-single mutants displayed similar mean GP values for the cell plate and the plasma membrane (Figure 7a,b), indicating similar lipid order. Hence, DRP1A localization not only depends on sterol composition, but its activity may also feedback on the lipid order of cell-plate membranes.

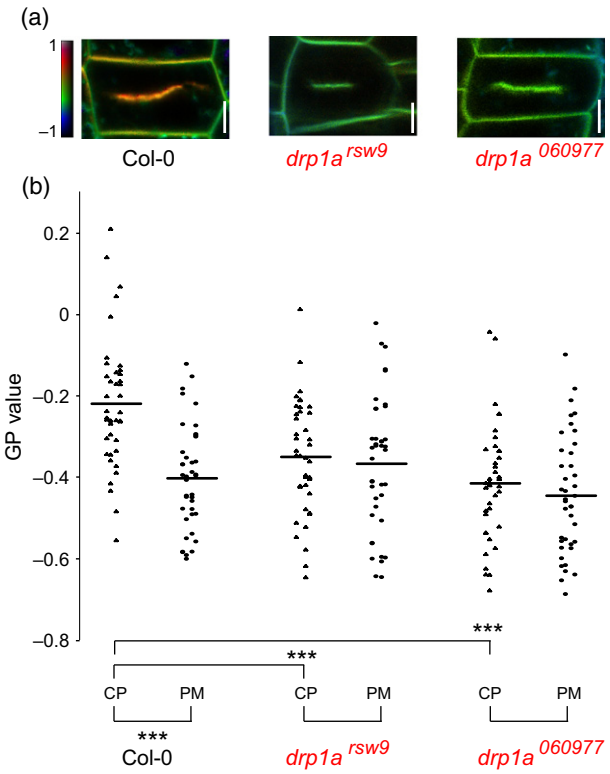

Figure 7. DRP1A is required for high membrane lipid order at the cell plate.
(a) Color-coded GP images from ratiometric fluorescence live imaging analyses of membrane lipid order in cytokinetic cells of 5-day-old seedling roots of genotypes Col-0, *drp1a*^{rsw9} or *drp1a*^{060977} labeled with di-4-ANEPPDHQ. Red, high lipid order; black, low lipid order.
(b) Quantitative analysis of mean GP value distributions from cell plates (CP) and plasma membranes (PM) obtained from multiple cells (n = 40) for each of the genotypes (Col-0, *drp1a*^{rsw9} or *drp1a*^{060977}) collected in 3–7 imaging experiments. Horizontal lines indicate means of the non-normal distributions. P values obtained using the non-parametric, two-tailed Mann–Whitney test with a significance threshold level at $P < 0.05$ indicate that differences between the indicated distributions are highly significant (***$P < 0.001$). Exact P values are given in Tables S2 and S3.
Note the strong difference in cell-plate membrane lipid order between Col-0 and *drp1a* mutant alleles.
The cells for Col-0 (n = 40) were acquired independently of the Col-0 cells for which results are shown in Figure 2c.

DISCUSSION

In this study, we provide evidence that the plant cell plate represents a high lipid-order membrane domain. Sterols are clearly present in cell-plate membranes but are not preferentially enriched here compared with the plasma membrane in cytokinetic cells. However, genetic and pharmacological interference with sterol biosynthesis strongly disrupted cell plate-specific membrane order (Figure 8). This suggests that additional, specifically localized components may contribute to membrane order. Strikingly, several CME components accumulate at the cell plate (Kang *et al.*, 2003a,b; Fujimoto *et al.*, 2007, 2008; Boutté *et al.*, 2010; Mravec *et al.*, 2011), and have been found to be enriched in DRMs from tobacco, *Nicotiana tabacum*, cells as well as Arabidopsis leaf plasma membranes (Mongrand *et al.*, 2004; Minami *et al.*, 2009). Indeed, we found that CME components were preferentially enriched in DRMs compared to non-DRMs from Arabidopsis root callus cultures, and observed that DRP1A, DRP2B and CLC2 co-localized with sterols at the cell plate in roots. Thus, sterol-rich, high lipid-order membranes apparently function as platforms for CME at the cell plate.

The stronger accumulation of DRP1A at the cell plate of *cpi1-1* mutant and fen-treated root cells compared to control roots, as well as the ectopic accumulation of YFP–KNOLLE and native KNOLLE at the plasma membrane of *cpi1-1* mutant and fen-treated seedlings during late cytokinesis, are consistent with the increased residence time of DRP1A foci at the cell cortex in elongated root cells of fen-treated roots (Konopka and Bednarek, 2008a). Thus, these

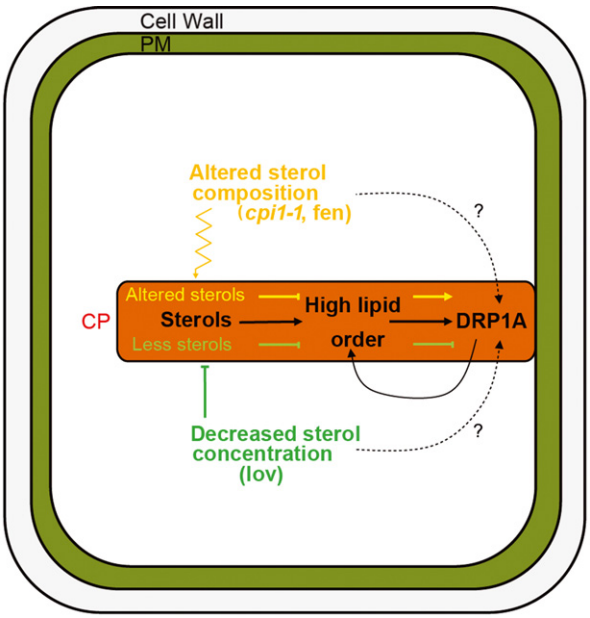

Figure 8. Model for sterol and DRP1A action on cell-plate membrane lipid order.
Alteration of sterol composition by *cpi1-1* mutation or fenpropimorph (fen) treatment induces a decrease in lipid order at the cell plate (CP) and increased DRP1A accumulation at the CP. The decreased sterol concentration caused by lovastatin (lov) treatment induces a decrease in lipid order at the CP and DRP1A residence at the CP. The lipid order of CP membranes is also decreased in the *drp1a* mutant, suggesting that DRP1A is needed for high lipid order. The mode(s) of sterol action on DRP1A requires further mechanistic analysis, and may include effects in addition to those on lipid order.

results suggest that alterations in sterol composition that induce accumulation of cyclopropylsterols affect the release of DRP1A from the membrane during endocytosis (Figure 8). By comparison, reduction of sterol concentration by lov treatment reduced the amount of DRP1A at the cell plate, but also decreased lipid membrane order, similar to alteration of sterol composition (Figure 8). This implies that a critical sterol concentration is required for high membrane order and DRP1A membrane localization. Collectively, our results indicate that DRP1A localization may be regulated by membrane sterol composition, although it is possible that alterations of sterol composition affect overall DRP1A protein abundance, because total DRP1A levels observed in protein extracts were affected similarly to DRP1A protein localization at the cell plate as observed by immunolocalization or use of fluorescent DRP1A fusion proteins. More intriguingly, DRP1A function itself is required for high membrane lipid order at the cell plate. Such potential feedback modulation of membrane lipid order by DRP1A may occur through its function in endocytosis. DRP1A function in endocytosis is required to restrict lateral diffusion of KNOLLE to the plane of cell division (Boutté *et al.*, 2010), as well as for selective asymmetric internalization of PIN auxin efflux carriers after cell division (Mravec *et al.*, 2011). Interestingly, sterols accumulate at the contractile actin ring in fission yeast and sea urchins during cytokinesis (Wachtler *et al.*, 2003; Takeda *et al.*, 2004; Ng *et al.*, 2005), and membrane raft components including dynamin are enriched in the mammalian midbody (Skop *et al.*, 2004). Our study on plants, which display a very different mode of cytokinesis, suggests that evolutionarily diverse organisms use high lipid-order membrane domains as platforms for execution of cytokinesis. Moreover, our findings provide precedence for a function of dynamin-like proteins in the lipid order of cytokinetic membranes. Future studies may reveal whether various eukaryotes employ dynamin-dependent endocytosis to create high lipid-order domains to drive execution of their diverse modes of cytokinesis.

EXPERIMENTAL PROCEDURES

Plant material and growth conditions

We used the *Arabidopsis thaliana* L. Heyn. ecotypes Landsberg *erecta* (L*er*) and Columbia-0 (Col-0), and the following mutants: *cpi1-1* in the L*er* background (Men *et al.*, 2008) and *cpi1-1* outcrossed seven times to the Col-0 background, herein referred to as *cpi1-1* in the Col-0 background, *drp1a*^{rsw9} (Collings *et al.*, 2008) and *drp1a*^{069077} (SALK_069077) in the Col-0 background (Collings *et al.*, 2008; Boutté *et al.*, 2010), *drp2a-1* and *drp2b-2* (Backues *et al.*, 2010), and *chc1-2*, *chc2-1* and *chc2-2* (Kitakura *et al.*, 2011) in the Col-0 background. Molecular characterization of the *cpi1-1*, *drp1a*, *drp2a-1*, *drp2b-2*, *chc1-2*, *chc2-1* and *chc2-2* mutants was performed by PCR-based genotyping as described previously (Collings *et al.*, 2008; Men *et al.*, 2008; Backues *et al.*, 2010; Boutté *et al.*, 2010; Kitakura *et al.*, 2011). In addition, we used the fluorescent protein marker lines *pKNOLLE:YFP-KNOLLE* in the L*er*/Niederzenz-0 background (El Kasmi *et al.*, 2013), *pDRP1A:DRP1A-tagRFP;pDRP2B:DRP2B-GFP* in the Col-0 background (Fujimoto *et al.*, 2010), and *pDRP1A:DRP1A-mGFP5* (Kang *et al.*, 2003a) and *pCLC2:CLC2-GFP* (Konopka and Bednarek, 2008b) in the Wassilewskija background. Plant growth conditions were as described previously (Fischer *et al.*, 2006). For DRM extraction and sterol analyses of root callus, 3-week-old callus cultures of L*er* and *cpi1-1* (in the L*er* background) were grown as described previously (Encina *et al.*, 2001) at 22°C, 60% humidity, in the dark.

Drug treatments

For inhibitor treatments, fenpropimorph (Pestanal, Sigma, http://www.sigmaaldrich.com/) was dissolved in DMSO to give a stock solution of 200 mg ml^{-1}, and lovastatin (Mevinolin, Sigma) was dissolved in DMSO to 2 mM, respectively. Seedlings were grown on MS agar plates containing 50 μg ml^{-1} fenpropimorph (fen) or 1 μM lovastatin (lov), or on control plates containing an equal amount of 0.1% DMSO. Analyses were performed on 5-day-old seedlings.

Sterol analysis from roots and root callus cultures of Arabidopsis

Sterol extraction and subsequent analysis of sterols derived from roots dissected from 5-day-old seedlings grown on MS

agar plates containing DMSO, 50 μg ml^{-1} fen or 1 μM lov was performed by GC/TOF MS exactly as previously described (Men *et al.*, 2008), except that five independent biological experiments were performed. Sterol analyses from root callus cultures were performed using 20 mg fresh weight of 3-week-old callus for each individual wild-type and mutant line tested.

Detergent-resistant membrane analysis

All steps of the DRM extraction were performed at 4°C as described previously (Borner *et al.*, 2005; Boutté *et al.*, 2010). In brief, root callus tissue derived from roots of 3-week-old L*er* or the *cpi1-1* mutant (in the L*er* background) was ground in two volumes of homogenization buffer (12% w/v sucrose, 100 mM Tris/HCl pH 8.0, 1 mM EDTA), and total membrane was collected as described previously (Borner *et al.*, 2005). Protein quantification was performed using a bicinchoninic acid (BCA) protein assay kit (Thermo Scientific, http://www.thermoscientific.com/) and a Spectra-MAX190 multichannel spectrophotometer (Molecular Devices, http://www.moleculardevices.com/). A total of 2.5 mg total membrane protein was incubated without Triton X-100 (ratio 0) or with 20 mg Triton X-100 (ratio 8) for 35 min under agitation (100 rpm). The final volume was kept constant for the two ratios so that the percentage of Triton X-100 did not exceed 3% at ratio 8. After sucrose step-gradient centrifugation, DRMs were collected as described previously (Borner *et al.*, 2005), and their protein concentration was determined using the BCA kit. Equal amounts of protein from various fractions (5–7 μg) were separated by SDS–PAGE using a Bio-Rad (http://www.bio-rad.com/) Mini-Protean® 3 system, and subjected to Western blotting. The primary antibodies and dilutions used were: rabbit anti-KNOLLE, 1:1000 (Lauber *et al.*, 1997); rabbit anti-SMT1, 1:100 (Agrisera, http://www.agrisera.com/) (Boutté *et al.*, 2010); rabbit anti-CLC2, 1:10 000 (Wang *et al.*, 2013); mouse anti-CHC-4A8, 1:1000 (ab33474, Abcam, http://www.abcam.com/); rabbit anti-DRP1A, 1:250 (Backues and Bednarek, 2010); rabbit anti-ARF1, 1:1000 (Agrisera). The secondary antibodies used were horseradish peroxidase-conjugated goat anti-mouse IgG, 1:3000 (Bio-Rad), and ECL horseradish peroxidase-linked donkey anti-rabbit IgG whole antibody, 1:10 000 (Amersham, http://www.gelifesciences.com/). An ECL Western blotting detection reagent kit (Amersham) was used for chemiluminescent detection.

Filipin-sterol fluorescence labeling and detection

Five-day-old seedlings were completely submerged in a filipin III (225 μM; Sigma)/4% w/v paraformaldehyde fixative solution in microtubule-stabilizing buffer (MTSB) comprising 50 mM PIPES, 5 mM EGTA, 5 mM $MgSO_4$, pH 7.0 (Grebe *et al.*, 2003). In a conventional microwave oven (Electrolux, http://www.electrolux.com), specimens were pulsed six or seven times for 30 sec at 90 W with an interval of at least 1 min between each pulse (Boutté *et al.*, 2011). Staining/fixation were continued for 1 h at room temperature in the dark, after which the seedlings were washed three times for 5 min each with sterile distilled water. In the case of co-labeling with CLC–GFP, the microwave step was omitted, and the seedlings were stained/fixed for 2 h at room temperature instead. Root tips were dissected and mounted in a drop of Citifluor AF1 (Citifluor Ltd, http://citifluor.com/). Fluorescence was detected by confocal laser scanning microscopy using a Leica TCS SP2 AOBS (http://www.leica-microsystems.com/) spectral system mounted on a Leica DM IRE2 inverted microscope. Image acquisition settings were as described previously (Boutté *et al.*, 2011). The excitation wavelengths used were 364 nm (argon UV laser) for filipin-sterol fluorescence, 488 nm (argon laser) for GFP and 561 nm (diode laser) for tagRFP (Figure S2). Fluorescence emission was detected between 400 and 484 nm, 492 and 557 nm and 580 and 700 nm, respectively. Pictures were overlaid and assembled using Adobe Illustrator CS6 (http://www.adobe.com/).

Ratiometric di-4-ANEPPDHQ fluorescence microscopy imaging of membrane lipid order

Di-4-ANEPPDHQ (D36802, Molecular Probes, http://www.lifetechnologies.com/) was dissolved in 300 μl DMSO to create a stock solution of 5 mM, and stored sealed in an air-tight, light-proof vial at room temperature (21°C) for up to 6 months. Staining solution was prepared by dissolving 2 μl of di-4-ANEPPDHQ stock solution in 2 ml of MS medium. Five-day-old seedlings were submerged in staining solution for 90 min at room temperature. Specimens were washed three times for 1 min at room temperature in MS medium, and roots were mounted for observation by confocal laser scanning microscopy using a Zeiss LSM 780 Axio Observer inverted microscope (http://www.zeiss.com/microscopy/en_de/home.html) and a water-corrected Plan-Apochromat 40×/1.20 DIC M27 objective (Zeiss; http://www.zeiss.com/microscopy/en_de/home.html). Di-4-ANEPPDHQ fluorescence was excited at 488 nm, and fluorescence intensity images were recorded simultaneously in the ranges 500–580 and 620–750 nm.

The calculation of the GP images obtained from ratiometric di-4-ANEPPDHQ fluorescence imaging was performed using ImageJ (http://imagej.nih.gov/ij/) following the procedure described by Owen *et al.* (2012) and using their custom-written macro. The ordered (500–580 nm) and disordered (620–750 nm) phase fluorescence channels were assigned ch00 and ch01, respectively. The threshold value for the analysis was fixed at 15, the color scale for the output GP images was set to 'grays', and no immunofluorescence mask was selected. The ImageJ macro for GP analysis generates GP images from ordered and disordered channel images based on the following equation:

$$GP = \frac{I_{500\_580} - GI_{620\_750}}{I_{500\_580} + GI_{620\_750}}$$

where *I* represents the intensity in each pixel in the image acquired in the indicated spectral channel (numbers in nm). To compensate for differences in the efficiency of collection in the two channels, GP values were corrected using a *G* factor. In order to obtain the *G* factor, the same microscope set-up employed for imaging root samples was used to image the fluorescence of a drop of undiluted di-4-ANEPPDHQ stock solution (2 μl) at three laser powers (0.3%, 0.5% and 1%). The mean pixel intensities of the channels ch00 (ordered) and ch01 (disordered) were extracted in ImageJ, and corresponding GP_{mes} values were calculated (using the previous equation with $G = 1$). The *G* factor was then calculated according to the equation:

$$G = \frac{GP_{ref} + GP_{ref}\ GP_{mes} - GP_{mes} - 1}{GP_{mes} + GP_{ref}\ GP_{mes} - GP_{ref} - 1}$$

GP_{ref} is a reference value for di-4-ANEPPDHQ in DMSO, here fixed at -0.85 (Owen *et al.*, 2012). In this study, the *G* factor was defined as $G = -0.35$.

GP values were calculated and pseudo-colored, ratiometric images were generated in ImageJ. The mean GP values were calculated for fluorescence at the cell plate (CP) and at the closest plasma membrane (PM) from cytokinetic root tip cells of Col-0 (two independent sets of cells, $n = 50$ and $n = 40$), *cpi1-1* (in the

Col-0 background) (n = 40), *drp1a*^{rsw9} (n = 40) and *drp1A*^{060977} (n = 40), as well as cells from Col-0 seedlings grown on plates containing 0.1% DMSO (n = 50), 50 μg ml^{-1} fen (n = 50 cells) or 1 μM lov (n = 50). As distributions of the measured populations of cells did not follow a normal distribution, the non-parametric, two-tailed Mann–Whitney *U* rank order sum test (http://elegans.som.vcu.edu/~leon/stats/utest.html) was used to test for significance of difference between the distribution of GP values of CP and PM. First, the difference between the distribution of GP values in the CP and PM was tested within the same line. Second, the difference between the distributions of GP values for the CP and GP values for the PM was compared between Col-0 and the mutant lines *cpi1-1* in the Col-0 background, *drp1a*^{rsw9} and *drp1A*^{060977}, or between Col-0 treated with DMSO and cells from seedlings treated with fen or lov.

Ratiometric PY3174 fluorescence microscopy imaging of membrane lipid order

PY3174 was employed using a similar procedure as for di-4-ANEPPDHQ. Stock solution for PY3174 (Kwiatek *et al.*, 2013) was prepared by dissolving 2 mg of the probe in ethanol to a final concentration of 6.57 mg ml^{-1}. Staining solution was prepared by dissolving 1 μl of PY3174 stock solution in 2 ml of MS medium. PY3174 fluorescence was excited at 488 nm, and fluorescence intensity images were recorded simultaneously in the ranges 505–590 and 620–690 nm. The ratiometric calculation of the GP images obtained from PY3174 fluorescence was performed as described above except that the *G* factor was defined as G = 0.82. The significance of the difference between the distribution of GP values for CP and PM was tested on n = 66 GP values each using a two-tailed Mann–Whitney *U* rank order sum test (http://elegans.som.vcu.edu/~leon/stats/utest.html).

Immunolocalization and confocal laser-scanning microscopy

Whole-mount immunofluorescence localization was performed as described previously (Fischer *et al.*, 2006; Men *et al.*, 2008; Boutté *et al.*, 2010). In brief, 5-day-old seedlings were fixed in 4% paraformaldehyde in MTSB for 1 h, then washed three times with MTSB, followed by three washes with sterile distilled water. Root tips were dissected, transferred to polylysine microscope slides (Menzel Gläser, http://www.menzel.de/), and dried at room temperature. Permeabilization was achieved by 35 min incubation in 2% Driselase (Sigma) at room temperature, followed by treatment for 1 h in 10% DMSO, 3% IPEGAL (Sigma) in MTSB (pH 7.0) at room temperature. After blocking with 5% normal donkey serum (Jackson ImmunoResearch, https://www.jacksonimmuno.com/) in MTSB, primary and secondary antibodies were applied. Washes were performed as described previously (Fischer *et al.*, 2006). Prior to mounting in Citifluor AF1, root tips were stained with 2 μg ml^{-1} 4′,6-diamidino-2-phenylindole (DAPI, Sigma) for 30 min. The primary antibodies and dilutions used were: rabbit anti-KNOLLE, 1:4000 (Lauber *et al.*, 1997) and rabbit anti-DRP1A, 1:500 (Backues and Bednarek, 2010). Secondary antibodies were diluted as follows: fluorescein isothiocyanate-coupled donkey anti-rabbit, 1:250 (Jackson ImmunoResearch), Cy5-coupled donkey anti-rabbit IgG, 1:300 (Jackson ImmunoResearch) and Dylight 649-conjugated affiniPure donkey anti-rabbit IgG (H+L), 1:800 (Jackson ImmunoResearch). Whole-mount immunolabeling detection and live imaging were performed by confocal laser scanning microscopy using either a Leica TCS SP2 AOBS spectral confocal laser scanning microscope mounted on a Leica DM IRE2 inverted microscope or a Zeiss LSM 780 Axio Observer inverted microscope. An oil-corrected 63× objective (NA = 1.4, HCX PL APO lbd.BL 63.0 × 1.40 oil; Leica) or a Plan-Apochromat 63×/1.40 oil DIC M27 in the Zeiss LSM 780, or a water-corrected 63× objective NA = 1.2 (HCX PL APO 63.0 × 1.20WBD UV, Leica) were used. Excitation wavelengths were 405 nm (blue diode laser) for DAPI, 488 nm for GFP and fluorescein isothiocyanate, 514 nm (argon laser) for YFP, 561 nm for tagRFP and 633 nm (helium/neon lasers) for Cy5/Dylight 649 fluorescence. Fluorescence emission was detected at 410–510 nm for DAPI, 490–595 nm for GFP (or 497–550 nm when imaged together with tagRFP), 500–550 nm for fluorescein isothiocyanate, 525–600 nm for YFP, 580–680 nm for tagRFP, 638-690 nm for Cy5, and 644–759 nm for Dylight 649. In multilabeling studies, detection was performed in sequential line-scanning mode with a line average of 8 for the Leica confocal laser scanning microscope or a line average of 4 for the Zeiss confocal laser scanning microscope. Pictures from sequential scans were overlaid and assembled using Adobe Illustrator CS6.

Quantitative analyses of fluorescence intensity

Transmitted light images obtained in parallel with DRP1A fluorescence enabled delineation of the cell plate in cells that had low levels of DRP1A label. Intensity measurements of DRP1A immunofluorescence or DRP1A–GFP were performed using ImageJ. The cell plate for each cytokinetic cell was encircled using the 'Polygon selection' tool, and the pixel intensity at the cell division plane was obtained using the 'histogram' option of the 'Analyze' menu. The mean pixel intensity was obtained by multiplying each intensity level (0–255) by the number of pixels displaying that corresponding intensity. Subsequently, the sum of all pixel intensity values was divided by the total number of pixels. Additionally, the same selection tool was used to define a region in the background, and the mean pixel intensity was measured in this area. For each cell, the mean pixel intensity at the cell division plane was corrected for background fluorescence. Values obtained were divided into classes, and these classes were plotted on a graph to obtain the distribution per genotype or treatment. Measurements were obtained for wild-type and *cpi1-1* mutant seedlings immunostained with anti-DRP1A antiserum. In addition, we quantified the DRP1A immunofluorescence in wild-type seedlings treated with fen, lov or DMSO, as described above. Furthermore, GFP fluorescence was quantified in DRP1A–GFP-expressing seedlings treated with fen, lov or DMSO. Statistical significances were calculated using the non-parametric two-tailed Mann–Whitney *U* rank order sum test (http://elegans.som.vcu.edu/~leon/stats/utest.html).

FRAP analyses

FRAP analyses were performed using a Zeiss LSM 780 Axio Observer inverted confocal laser scanning microscope with a water-corrected 40×/1.2 C-Apochromat M27 objective (Zeiss). Pre-bleach and post-bleach signals of YFP–KNOLLE fluorescence were detected at 1% laser power for the 514 nm laser excitation line and 510–620 nm emission settings. One bleach frame of 2 μm diameter at the membrane was placed in the middle of the cell division plane. Photobleaching was performed using ten 3.64 s bleach scan periods and 100% main laser power for the 514 nm excitation laser line. Values from the plane of cell division were normalized for loss of fluorescence caused by photobleaching by correcting for differences between pre- and post-bleach values observed in neighboring cells. For each treatment condition, 13 cells from 13 individual roots were analyzed. Values were normalized to pre-bleach values and post-bleach values corresponding to 100% and 0%, respectively. The half-time ($t_{½}$) required for fluorescence in the photobleached region to recover to 50% of the recovery asymptote was 15 min. The significance of the subtle deviations observed between

DMSO- and lov-treated cell populations analyzed by FRAP was determined using Student's two-tailed, two-sample *t* test assuming equal variance.

Western blot analysis of total protein extracts

Total protein was extracted from 5-day-old seedlings grown on MS agar plates containing 50 μg ml^{-1} fen or 1 μM lov, or control plates containing an equal volume of 0.1% DMSO compared to the fen- and lov-containing plates. Seedlings were frozen in liquid nitrogen and ground with a fine pestle in 200 μl extraction buffer per 20 seedlings. The extraction buffer comprised 25 mM Tris/HCl pH 7.5, 10 mM $MgCl_2$, 5 mM EGTA, 10% glycerol, 100 mM NaCl, 0.2% Tween-20, 10 μl ml^{-1} proteinase inhibitor cocktail (Sigma Aldrich) and 2 mM dithiothreitol. Supernatants were collected after 10 min centrifugation at 11 000 *g*, and used for Western blot analyses. Protein quantification was performed using Bradford reagent (Bio-Rad). Equal amounts of protein (30 μg) were separated by SDS–PAGE using a Bio-Rad Mini-Protean® 3 system, and subjected to Western blotting. The primary antibodies and dilutions used were: mouse monoclonal anti-Hsc70 antibody and plant ER BiP (endoplasmic reticulum Binding Protein), 1:1000 (Nordic Biosite AB, http://www.nordicbiosite.com/), rabbit anti-DRP1A, 1:500 (Backues and Bednarek, 2010) and rabbit anti-KNOLLE, 1:1000 (Lauber *et al.*, 1997). The secondary antibodies were horseradish peroxidase-conjugated goat anti-mouse IgG (Bio-Rad), 1:3000 and horseradish peroxidase-linked ECL donkey anti-rabbit IgG whole antibody, 1:10000 (Amersham). An ECL Western blotting detection reagent kit (Amersham) was used for chemiluminescent detection.

ACCESSION NUMBERS

The Arabidopsis Genome Initiative or GenBank/EMBL database accession numbers for the sequences referred to in this paper are At5g50375 (*CPI1*), At5g42080 (*DRP1A*), At1g59610 (*DRP2B*), At3g08530 (*CHC2*), At3g11130 (*CHC1*), At2g40060 (*CLC2*), At1g23490 (*ARF1*) and At5g13710 (*SMT1*).

ACKNOWLEDGMENTS

We are grateful to Jirí Friml (Institute of Science and Technology Austria, Klosterneuburg, Austria) Nobuhiro Tsutsumi (Department of Agricultural and Environmental Biology, University of Tokyo, Japan) and Richard E. Williamson (Research School of Biological Sciences, Australian National University, Canberra, Australia) for sharing published materials and reagents. We thank Dylan M. Owen (Experimental Biophysics & Nanotechnology, King's College London, UK) for helpful advice on ratiometric lipid-order imaging, and Stéphanie Robert for critical reading of the manuscript. We thank the Nottingham Arabidopsis Stock Centre for providing seed stocks. This work was supported by the Swedish Research Council for the Environment, Agricultural Sciences and Spatial Planning (Formas) (grant number 2007-715 to M.G.), a postdoctoral stipend from the Carl Tryggers Foundation for T.S. to M.G., a US National Science Foundation award (number 1121998) to S.Y.B., and a grant from the Swedish Kempe Foundations to M.G.

SUPPORTING INFORMATION

Additional Supporting Information may be found in the online version of this article.

Figure S1. Cell-plate lipid-order analysis using the membrane order-sensitive probe PY3174.

Figure S2. Effects of CME gene mutations on KNOLLE localization, and effects of sterol biosynthesis interference on CME component localization.

Figure S3. Lovastatin effects on YFP–KNOLLE lateral diffusion determined by FRAP analysis.

Figure S4. Differential effects of lovastatin and fenpropimorph treatments on DRP1A total protein levels.

Table S1. Statistical analyses of differences in relative GP values between different cell-plate maturation stages during cytokinesis.

Table S2. Statistical analyses of differences between GP value distributions of cell plates and plasma membranes from various genotypes or treatments.

Table S3. Statistical analyses of differences between GP value distributions from cell plates or plasma membranes from mutants or treatments compared to wild-type or mock-treated controls.

REFERENCES

Atilla-Gokcumen, G.E., Muro, E., Relat-Goberna, J., Sasse, S., Bedigian, A., Coughlin, M.L., Garcia-Manyes, S. and Eggert, U.S. (2014) Dividing cells regulate their lipid composition and localization. *Cell*, **156**, 428–439.

Bach, T.J. and Lichtenthaler, H.K. (1983) Mechanisms of inhibition by mevinolin (MK 803) of microsome-bound radish and of partially purified yeast HMG-CoA reductase (EC.1.1.1.34). *Z. Naturforsch. C* **38**, 212–219.

Backues, S.K. and Bednarek, S.Y. (2010) Arabidopsis dynamin-related protein 1A polymers bind, but do not tubulate, liposomes. *Biochem. Biophys. Res. Commun.* **393**, 734–739.

Backues, S.K., Korasick, D.A., Heese, A. and Bednarek, S.Y. (2010) The Arabidopsis dynamin-related protein2 family is essential for gametophyte development. *Plant Cell*, **22**, 3218–3231.

Barr, F.A. and Grüneberg, U. (2007) Cytokinesis: placing and making the final cut. *Cell*, **131**, 847–860.

Borner, G.H., Sherrier, D.J., Weimar, T., Michaelson, L.V., Hawkins, N.D., Macaskill, A., Napier, J.A., Beale, M.H., Lilley, K.S. and Dupree, P. (2005) Analysis of detergent-resistant membranes in Arabidopsis. Evidence for plasma membrane lipid rafts. *Plant Physiol.* **137**, 104–116.

Boutté, Y., Frescatada-Rosa, M., Men, S. *et al.* (2010) Endocytosis restricts Arabidopsis KNOLLE syntaxin to the cell division plane during late cytokinesis. *EMBO J.* **29**, 546–558.

Boutté, Y., Men, S. and Grebe, M. (2011) Fluorescent in situ visualization of sterols in Arabidopsis roots. *Nat. Protoc.* **6**, 446–456.

Collings, D.A., Gebbie, L.K., Howles, P.A., Hurley, U.A., Birch, R.J., Cork, A.H., Hocart, C.H., Arioli, T. and Williamson, R.E. (2008) Arabidopsis dynamin-like protein DRP1A: a null mutant with widespread defects in endocytosis, cellulose synthesis, cytokinesis, and cell expansion. *J. Exp. Bot.* **59**, 361–376.

El Kasmi, F., Krause, C., Hiller, U., Stierhof, Y.D., Mayer, U., Conner, L., Kong, L., Reichardt, I., Sanderfoot, A.A. and Jürgens, G. (2013) SNARE complexes of different composition jointly mediate membrane fusion in Arabidopsis cytokinesis. *Mol. Biol. Cell* **24**, 1593–1601.

Encina, C.L., Constantin, M. and Botella, J. (2001) An easy and reliable method for establishment and maintenance of leaf and root cell cultures of *Arabidopsis thaliana*. *Plant Mol. Biol. Rep.* **19**, 245–248.

Fernandez, C., Lobo Md Mdel, V., Gomez-Coronado, D. and Lasuncion, M.A. (2004) Cholesterol is essential for mitosis progression and its deficiency induces polyploid cell formation. *Exp. Cell Res.* **300**, 109–120.

Fischer, U., Ikeda, Y., Ljung, K., Serralbo, O., Singh, M., Heidstra, R., Palme, K., Scheres, B. and Grebe, M. (2006) Vectorial information for Arabidopsis planar polarity is mediated by combined AUX1, EIN2, and GNOM activity. *Curr. Biol.* **16**, 2143–2149.

Fujimoto, M., Arimura, S., Nakazono, M. and Tsutsumi, N. (2007) Imaging of plant dynamin-related proteins and clathrin around the plasma membrane by variable incidence angle fluorescence microscopy. *Plant Biotechnol.* **24**, 449–455.

Fujimoto, M., Arimura, S., Nakazono, M. and Tsutsumi, N. (2008) Arabidopsis dynamin-related protein DRP2B is co-localized with DRP1A on the leading edge of the forming cell plate. *Plant Cell Rep.* **27**, 1581–1586.

Fujimoto, M., Arimura, S., Ueda, T., Takanashi, H., Hayashi, Y., Nakano, A. and Tsutsumi, N. (2010) Arabidopsis dynamin-related proteins DRP2B

and DRP1A participate together in clathrin-coated vesicle formation during endocytosis. *Proc. Natl Acad. Sci. USA* **107**, 6094–6099.

Gerbeau-Pissot, P., Der, C., Thomas, D., Anca, I.A., Grosjean, K., Roche, Y., Perrier-Cornet, J.M., Mongrand, S. and Simon-Plas, F. (2013) Modification of plasma membrane organization in tobacco cells elicited by cryptogein. *Plant Physiol.* **164**, 273–286.

Grebe, M., Xu, J., Möbius, W., Ueda, T., Nakano, A., Geuze, H.J., Rook, M.B. and Scheres, B. (2003) Arabidopsis sterol endocytosis involves actin-mediated trafficking via ARA6-positive early endosomes. *Curr. Biol.* **13**, 1378–1387.

He, J.X., Fujioka, S., Li, T.C., Kang, S.G., Seto, H., Takatsuto, S., Yoshida, S. and Jang, J.C. (2003) Sterols regulate development and gene expression in Arabidopsis. *Plant Physiol.* **131**, 1258–1269.

Ito, E., Fujimoto, M., Ebine, K., Uemura, T., Ueda, T. and Nakano, A. (2012) Dynamic behavior of clathrin in *Arabidopsis thaliana* unveiled by live imaging. *Plant J.* **69**, 204–216.

Jin, L., Millard, A.C., Wuskell, J.P., Dong, X., Wu, D., Clark, H.A. and Loew, L.M. (2006) Characterization and application of a new optical probe for membrane lipid domains. *Biophys. J.* **90**, 2563–2575.

Jürgens, G. (2005) Cytokinesis in higher plants. *Annu. Rev. Plant Biol.* **56**, 281–299.

Kang, B.H., Busse, J.S. and Bednarek, S.Y. (2003a) Members of the Arabidopsis dynamin-like gene family, ADL1, are essential for plant cytokinesis and polarized cell growth. *Plant Cell*, **15**, 899–913.

Kang, B.H., Rancour, D.M. and Bednarek, S.Y. (2003b) The dynamin-like protein ADL1C is essential for plasma membrane maintenance during pollen maturation. *Plant J.* **35**, 1–15.

Kitakura, S., Vanneste, S., Robert, S., Löfke, C., Teichmann, T., Tanaka, H. and Friml, J. (2011) Clathrin mediates endocytosis and polar distribution of PIN auxin transporters in Arabidopsis. *Plant Cell*, **23**, 1920–1931.

Konopka, C.A. and Bednarek, S.Y. (2008a) Comparison of the dynamics and functional redundancy of the Arabidopsis dynamin-related isoforms DRP1A and DRP1C during plant development. *Plant Physiol.* **147**, 1590–1602.

Konopka, C.A. and Bednarek, S.Y. (2008b) Variable-angle epifluorescence microscopy: a new way to look at protein dynamics in the plant cell cortex. *Plant J.* **53**, 186–196.

Kwiatek, J.M., Owen, D.M., Abu-Siniyeh, A., Yan, P., Loew, L.M. and Gaus, K. (2013) Characterization of a new series of fluorescent probes for imaging membrane order. *PLoS ONE*, **8**, e52960.

Lauber, M.H., Waizenegger, I., Steinmann, T., Schwarz, H., Mayer, U., Hwang, I., Lukowitz, W. and Jürgens, G. (1997) The Arabidopsis KNOLLE protein is a cytokinesis-specific syntaxin. *J. Cell Biol.* **139**, 1485–1493.

Lingwood, D. and Simons, K. (2007) Detergent resistance as a tool in membrane research. *Nat. Protoc.* **2**, 2159–2165.

Liu, P., Li, R.L., Zhang, L., Wang, Q.L., Niehaus, K., Baluska, F., Samaj, J. and Lin, J.X. (2009) Lipid microdomain polarization is required for NADPH oxidase-dependent ROS signaling in Picea meyeri pollen tube tip growth. *Plant J.* **60**, 303–313.

McMichael, C.M., Reynolds, G.D., Koch, L.M., Wang, C., Jiang, N., Nadeau, J., Sack, F.D., Gelderman, M.B., Pan, J. and Bednarek, S.Y. (2013) Mediation of clathrin-dependent trafficking during cytokinesis and cell expansion by Arabidopsis stomatal cytokinesis defective proteins. *Plant Cell*, **25**, 3910–3925.

Men, S., Boutté, Y., Ikeda, Y., Li, X., Palme, K., Stierhof, Y.D., Hartmann, M.A., Moritz, T. and Grebe, M. (2008) Sterol-dependent endocytosis mediates post-cytokinetic acquisition of PIN2 auxin efflux carrier polarity. *Nat. Cell Biol.* **10**, 237–244.

Minami, A., Fujiwara, M., Furuto, A., Fukao, Y., Yamashita, T., Kamo, M., Kawamura, Y. and Uemura, M. (2009) Alterations in detergent-resistant plasma membrane microdomains in *Arabidopsis thaliana* during cold acclimation. *Plant Cell Physiol.* **50**, 341–359.

Mongrand, S., Morel, J., Laroche, J., Claverol, S., Carde, J.P., Hartmann, M.A., Bonneu, M., Simon-Plas, F., Lessire, R. and Bessoule, J.J. (2004) Lipid rafts in higher plant cells: purification and characterization of Triton X-100-insoluble microdomains from tobacco plasma membrane. *J. Biol. Chem.* **279**, 36277–36286.

Mravec, J., Petrasek, J., Li, N. *et al.* (2011) Cell plate restricted association of DRP1A and PIN proteins is required for cell polarity establishment in Arabidopsis. *Curr. Biol.* **21**, 1055–1060.

Ng, M.M., Chang, F. and Burgess, D.R. (2005) Movement of membrane domains and requirement of membrane signaling molecules for cytokinesis. *Dev. Cell* **9**, 781–790.

Owen, D.M., Lanigan, P.M., Dunsby, C., Munro, I., Grant, D., Neil, M.A., French, P.M. and Magee, A.I. (2006) Fluorescence lifetime imaging provides enhanced contrast when imaging the phase-sensitive dye di–4–ANEPPDHQ in model membranes and live cells. *Biophys. J.* **90**, L80–L82.

Owen, D.M., Rentero, C., Magenau, A., Abu-Siniyeh, A. and Gaus, K. (2012) Quantitative imaging of membrane lipid order in cells and organisms. *Nat. Protoc.* **7**, 24–35.

Pike, L.J. (2006) Rafts defined: a report on the Keystone Symposium on Lipid Rafts and Cell Function. *J. Lipid Res.* **47**, 1597–1598.

Prekeris, R. and Gould, G.W. (2008) Breaking up is hard to do - membrane traffic in cytokinesis. *J. Cell Sci.* **121**, 1569–1576.

Roche, Y., Gerbeau-Pissot, P., Buhot, B., Thomas, D., Bonneau, L., Gresti, J., Mongrand, S., Perrier-Cornet, J.M. and Simon-Plas, F. (2008) Depletion of phytosterols from the plant plasma membrane provides evidence for disruption of lipid rafts. *FASEB J.* **22**, 3980–3991.

Samuels, A.L., Giddings, T.H. Jr and Staehelin, L.A. (1995) Cytokinesis in tobacco BY-2 and root tip cells: a new model of cell plate formation in higher plants. *J. Cell Biol.* **130**, 1345–1357.

Simons, K. and Sampaio, J.L. (2011) Membrane organization and lipid rafts. *Cold Spring Harb. Perspect. Biol.* **3**, 1–17.

Skop, A.R., Liu, H., Yates, J. 3rd, Meyer, B.J. and Heald, R. (2004) Dissection of the mammalian midbody proteome reveals conserved cytokinesis mechanisms. *Science*, **305**, 61–66.

Takeda, T., Kawate, T. and Chang, F. (2004) Organization of a sterol-rich membrane domain by cdc15p during cytokinesis in fission yeast. *Nat. Cell Biol.* **6**, 1142–1144.

Wachtler, V., Rajagopalan, S. and Balasubramanian, M.K. (2003) Sterol-rich plasma membrane domains in the fission yeast Schizosaccharomyces pombe. *J. Cell Sci.* **116**, 867–874.

Wang, C., Yan, X., Chen, Q., Jiang, N., Fu, W., Ma, B., Liu, J., Li, C., Bednarek, S.Y. and Pan, J. (2013) Clathrin light chains regulate clathrin-mediated trafficking, auxin signaling, and development in Arabidopsis. *Plant Cell*, **25**, 499–516.

Xu, J. and Scheres, B. (2005) Dissection of Arabidopsis ADP-RIBOSYLATION FACTOR 1 function in epidermal cell polarity. *Plant Cell*, **17**, 525–536.

Xu, X., Bittman, R., Duportail, G., Heissler, D., Vilcheze, C. and London, E. (2001) Effect of the structure of natural sterols and sphingolipids on the formation of ordered sphingolipid/sterol domains (rafts). Comparison of cholesterol to plant, fungal, and disease-associated sterols and comparison of sphingomyelin, cerebrosides, and ceramide. *J. Biol. Chem.* **276**, 33540–33546.